JACS
JOURNAL OF THE AMERICAN CHEMICAL SOCIETY

Article

pubs.acs.org/JACS

Improving the Efficiency and Activity of Electrocatalysts for the Reduction of CO_2 through Supramolecular Assembly with Amino Acid-Modified Ligands

Charles W. Machan,[†] Jian Yin,[‡] Steven A. Chabolla,[†] Michael K. Gilson,[‡] and Clifford P. Kubiak*[,†]

[†]Department of Chemistry and Biochemistry, University of California − San Diego, 9500 Gilman Drive 0358, La Jolla, California 92023, United States

[‡]Skaggs School of Pharmacy and Pharmaceutical Sciences, University of California − San Diego, 9500 Gilman Drive, La Jolla, California 92093-0736, United States

Supporting Information

ABSTRACT: The use of hydrogen-bonding interactions to direct the noncovalent assembly of a Re-based bimetallic supramolecular electrocatalyst containing either tyrosine or phenylalanine residues is reported. Computational modeling and spectroelectrochemical characterization indicate that under catalytic conditions the phenol residues of tyrosine can act both as pendant proton sources and participate in the structural assembly of the bimetallic active species. As a result, an increased rate of catalysis is observed experimentally for the reductive disproportionation of CO_2 to CO and CO_3^{2-} by a tyrosine-modified complex in comparison to a control complex containing phenylalanine residues. These findings demonstrate that noncovalent assembly is a powerful method for generating new bimetallic electrocatalyst systems where the choice of substituent can be used to both control structural assembly and introduce cocatalytic moieties.

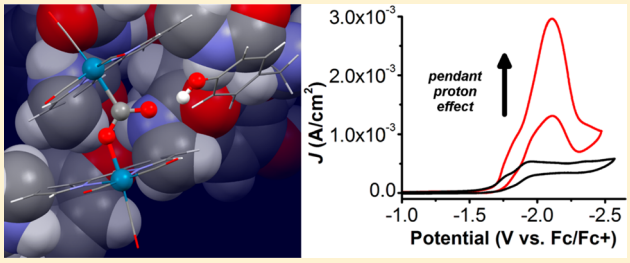

INTRODUCTION

The efficient electrocatalytic conversion of carbon dioxide (CO_2) to fuels and commodity chemicals represents a continuing challenge for the storage of electrical energy from renewable sources in chemical bonds.[1−5] Some of the most effective CO_2 reduction electrocatalysts are based on the Group VII bipyridine *fac*-tricarbonyl complexes Re^{I}(2,2′-bipyridine)$(CO)_3Cl$ [2,2′-bipyridine = bpy] and Mn^{I}(2,2′-bipyridine)$(CO)_3X$ [X = Br and OTf], which form carbon monoxide (CO) and water (H_2O) with near perfect Faradaic efficiency via a unimolecular $[M(bpy)]^{-}/2e^{-}$ pathway.[6−18] Interestingly, Re(bpy) compounds can also reduce CO_2 via a bimolecular $2[Re(bpy)]/[1e^{-} + 1e^{-}]$ pathway, producing CO and carbonate (CO_3^{2-}).[19−21] We recently reported that the modification of the bipyridine ligand with methyl acetamidomethyl groups at the 4 and 4′ positions, to create Re((4,4′-bis(methyl acetamidomethyl)-2,2′-bipyridine)$(CO)_3Cl$, [Re(**dac**)CO_3Cl], promotes this mechanism in acetonitrile (MeCN).[22] Computational models, electrochemical measurements, and infrared spectroelectrochemistry (IR-SEC), revealed that the bimolecular catalytic response resulted from the supramolecular assembly of a dimer species through hydrogen bonding.

These results led us to ask whether the supramolecular catalyst system could be further improved, in terms of current efficiency and turnover frequency (TOF), through the incorporation of biomimetic components, such as amino acid residues. This idea is inspired by nature, specifically metalloproteins, which place active sites and cocatalytic residues in close proximity.[23−25] In these systems, the inherent flexibility of the noncovalent interactions which direct the formation of the higher-order structure accommodates a variety of conformational changes during the course of a reaction. Indeed, amino acids have been successfully incorporated into a variety of H_2 oxidation, formate oxidation, and proton reduction electrocatalysts.[26−30] Amino acids and peptides are attractive for use in the outer-sphere of molecular catalysts because they can be used to alter activity by introducing pH responsiveness, changing solubility, and forming beneficial secondary structures.[31−33] Related but parallel efforts have focused on the incorporation of proton relays in molecular electrocatalysts for proton-dependent transformations of CO_2 for both Mn(bpy)[34,35] and tetra-aryl Fe porphyrin derivatives.[36−38] We reasoned that adding amino acid residues to the previously reported Re(bpy)-based dimer catalyst system might improve the activity by increasing the stability of the bimetallic active state and incorporating pendant proton sources.[22,28,32−36,39,40] The results of this investigation indicate that the addition of tyrosine residues promotes the formation of a more stable bimetallic active species and increased current efficiency over Re(**dac**)CO_3Cl.

Received: April 12, 2016
Published: June 3, 2016

DOI: 10.1021/jacs.6b03774
J. Am. Chem. Soc. 2016, 138, 8184−8193

Scheme 1. Synthesis of Re(Tyrdac)$(CO)_3$Cl and Re(Phedac)$(CO)_3$Cl[a]

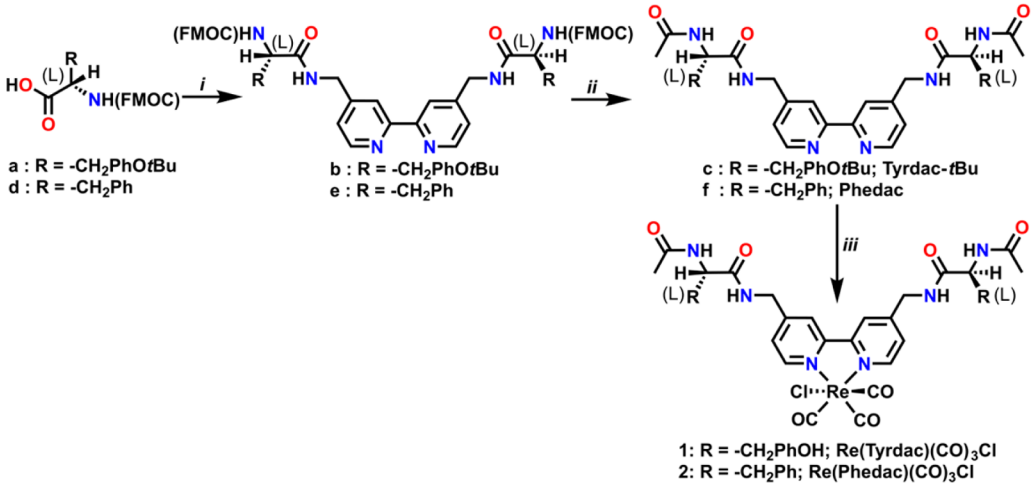

[a](i) 1 equiv each of *N*-hydroxysuccinimide, triphenylamine, and *N*,*N*-diisopropylcarbodiimide in CH_2Cl_2, 1 h; 0.5 equiv of 4,4′-bis(methylamine)-2,2′-bipyridine, 3 h. (ii) 2.1 equiv of 4-methylpiperidine in CH_2Cl_2 or *N*,*N*-DMF, 1 h; 2.1 equiv each of acetic anhydride and triethylamine, 1 h. (iii) 1 equiv of $Re(CO)_5Cl$ in toluene, reflux 3 h; the *t*Bu protecting group for **1** was removed by then suspended in a 95:5 trifluoroacetic acid:CH_2Cl_2 mixture (~5 mL) for 20 min before being precipitated with excess diethyl ether.

RESULTS

Synthesis and Characterization. A *tert*-butyl protected tyrosine-functionalized (tyrosine = Tyr) bpy ligand (*N*,*N*′-([2,2′-bipyridine]-4,4′-diylbis(methylene))bis(2-acetamido-3-(4-(*tert*-butoxy)phenyl)propanamide = **Tyrdac-*t*Bu**), was synthesized via the preparation of an NHS-ester from FMOC-L-Tyr(O*t*Bu)-OH and subsequent coupling with 0.5 equiv of 4,4′-bis(methylamine)-2,2′-bipyridine. The FMOC protecting groups were removed with 4-methylpiperidine and the resulting primary amine was immediately acylated with acetic anhydride in situ. After purification this *tert*-butyl protected Tyr-based ligand was heated to reflux with rhenium pentacarbonyl chloride [$Re(CO)_5Cl$] in toluene for 3 h and the resulting yellow solution condensed under a vacuum. The isolated solid was suspended in trifluoroacetic acid with minimal CH_2Cl_2 for 1 h to remove the *tert*-butyl protecting groups before an excess of diethyl ether (Et_2O) was added to induce precipitation. This filtrate was dissolved in acetonitrile (MeCN) and filtered through Celite whereupon the solvent was removed under reduced pressure and Re(**Tyrdac**)$(CO)_3$Cl, **1**, was isolated as a yellow powder. This solid material was characterized by NMR and IR spectroscopies, ESI-MS, and microanalysis, as consistent with the proposed structure of **1** (Scheme 1). The corresponding control compound with L-phenylalanine (Phe) was prepared in a similar manner, Re(**Phedac**)$(CO)_3$Cl, **2** (Scheme 1, see Experimental Section).

Initial Characterization of the Electrochemical Behavior of Re(Tyrdac)$(CO)_3$Cl. Electrochemical studies of complex **1** in MeCN (1 mM in 0.1 M tetrabutylammonium hexafluorophosphate [$TBAPF_6$]/MeCN) revealed four reduction features at negative potentials, similar to the previously characterized Re(**dac**)CO_3Cl system.[15,16,18] The first wave at −1.77 V is chemically irreversible, the second at −1.96 V is also chemically irreversible, followed by a quasi-reversible feature at −2.06 V (E_{pc}), and a final irreversible feature at −2.25 V (vs Fc/Fc+, Figure 1). A simplified depiction of the proposed reduction mechanism is found in Scheme 2.

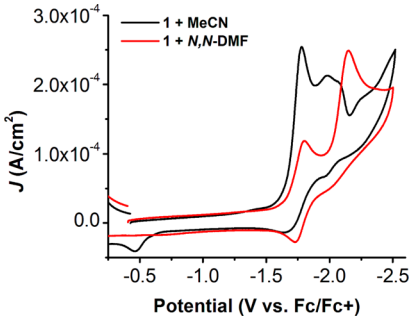

Figure 1. CVs of Re(**Tyrdac**)$(CO)_3$Cl (**1**) under Ar saturation conditions in MeCN (black) and *N*,*N*-DMF (red). Conditions: 1 mM in 0.1 $TBAPF_6$/MeCN or *N*,*N*-DMF; glassy carbon working electrode, Pt wire counter electrode, Ag/AgCl pseudoreference electrode; referenced to internal Fc standard; scan rate 100 mV/s.

Scheme 2. Simplified Reduction Mechanism of Hydrogen-Bonded Re(bpy) Dimers

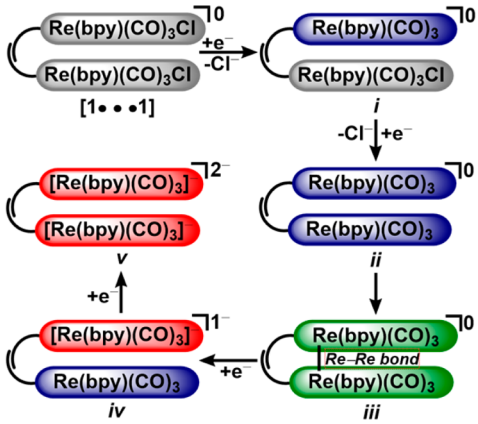

On the basis of prior characterization of Re(**dac**)CO_3Cl and the IR-SEC data detailed below, we assign the first two reductive processes to the stepwise reduction of a hydrogen-bonded dimer [**1**···**1**], where only one equiv of **1** in the dimer is

DOI: 10.1021/jacs.6b03774
J. Am. Chem. Soc. 2016, 138, 8184−8193

reduced at a time due to the formation of a stable mixed-valence state (i). The proposed bimolecular active state forms after the second reduction process (ii) and is in competition with the formation of a metal−metal bond that generates $[Re(\mathbf{Tyrdac})(CO)_3]_2$ (iii). The following two reduction features correspond to the stepwise reduction and cleavage of the metal−metal bond in $[Re(\mathbf{Tyrdac})(CO)_3]_2$ (iv and v). Consistent with this interpretation, an irreversible oxidation feature is observed at −0.47 V (vs Fc/Fc+) on the return sweep, which is assigned to the oxidation of $[Re(\mathbf{Tyrdac})(CO)_3]_2$. Variable-scan rate studies showed that these reduction features persist to 3200 mV/s, a scan rate where previous experiments showed that the rate of dimerization for $Re(\mathbf{dac})CO_3Cl$ was too slow for observation at this experimental time scale (Figure S1).[22] On the basis of the difference in potential of the first two redox features, we estimate the value of the comproportionation constant, K_c, of **1** to be 1.58×10^3, an increase from $Re(\mathbf{dac})CO_3Cl$ (K_c = 340). The unitless value K_c corresponds to the stability of the mixed-valent state relative to the two isovalent states, with larger values indicating greater stability from electron delocalization.[41] When **1** is instead solvated in *N*,*N*-DMF (Figure 1) the reduction features resolve from four to two and the oxidation corresponding to the Re−Re bonded dimer disappears, suggesting that the hydrogen-bonding interactions have been disrupted by competitive interactions, vide infra.[22]

A CO_2-saturated solution of complex **1** shows an increase in current at the second of the four redox features, which is consistent with a catalytic response (peak current, E_{pc}, at −2.11 V vs Fc/Fc+, Figure 2; Scheme 3). With the addition of phenol

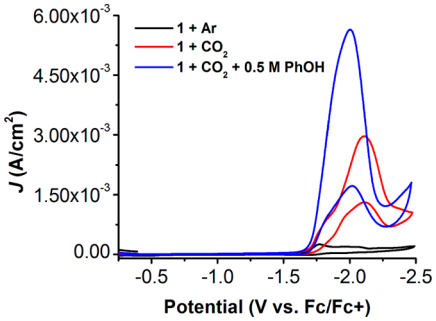

Figure 2. CVs of the current response of $Re(\mathbf{Tyrdac})(CO)_3Cl$ (**1**) at negative potentials under Ar saturation conditions (black), CO_2 saturation (red), and CO_2 saturation with added PhOH (0.5 M; blue). Conditions: 1 mM in 0.1 $TBAPF_6$/MeCN; glassy carbon working electrode, Pt wire counter electrode, Ag/AgCl pseudoreference electrode; referenced to internal Fc standard; scan rate 100 mV/s.

(PhOH, 0.5 M) the current density approximately doubles, and E_{pc} shifts to slightly more positive potentials: −2.00 V vs Fc/Fc+. Bulk electrolysis experiments at −2.2 V vs Fc/Fc+ showed 99 ± 7% current efficiency for the formation of CO through 6.0 turnovers (2 ± 0.024% current efficiency for H_2), based on the moles of **1** in solution.[15−18] Using the ratio of catalytic current to Faradaic (i_{cat}/i_p), which is proportional to the electrocatalytic rate constant and TOF, it is possible to approximate a theoretical maximum TOF for CO_2 saturation with and without added PhOH (see Supporting Information for details).[17,42−44] To apply to this system, however, we need to assume that we can treat the hydrogen-bonded dimer as a first-order catalyst and that the slowest step of the reaction is the hydrogen-bonded dimer reacting with CO_2, such that the peak catalytic current achieved (i_{cat}) will represent the slowest reaction rate.[22,42] With these assumptions, the *maximum* theoretical TOF for **1** under CO_2 saturation is 46 s^{-1} and 170 s^{-1} under CO_2 saturation with added PhOH (0.5 M). The highest TOFs estimated for $Re(\mathbf{dac})(CO)_3Cl$ with CO_2 saturation were 19 s^{-1} and 57 s^{-1} with added trifluoroethanol (0.795 M).[22] Variable scan-rate experiments from 100 mV/s to 3200 mV/s under CO_2 saturation showed a decreased shift in E_{pc} to more negative potentials for **1** than what had been observed previously for $Re(\mathbf{dac})CO_3Cl$ (**1**: −2.11 V to −2.18 V; $Re(\mathbf{dac})(CO_3)Cl$: −1.98 V to −2.33 V vs Fc/Fc+; Figure S2). This decreased shift for E_{pc} suggests that the increased stability of the dimer observed under Faradaic conditions for **1** is retained under catalytic conditions.

These experiments were repeated in *N*,*N*-DMF to examine the effects of disrupting the hydrogen-bonding interactions.[22] Under Ar saturation in *N*,*N*-DMF complex **1** showed a much different response by CV compared to the voltammograms obtained in MeCN (Figure 1). Only two reduction waves were observed on the forward sweep to negative potentials: a quasi-reversible wave at $E_{1/2}$ = −1.77 V (ΔE_p = 70 mV) and an irreversible one at −2.15 V vs Fc/Fc+. On the basis of prior reports, these waves are assigned to the unimolecular first and second reductions of **1**, respectively, which generate the five-coordinate anion $[Re(\mathbf{Tyrdac})(CO)_3]^-$. The absence of an oxidation feature corresponding to $[Re(\mathbf{Tyrdac})(CO)_3]_2$ on the return sweep supports this assignment. Under CO_2 saturation an increase in current is observed at the second reduction, indicative of catalysis by **1** via a unimolecular $[Re(bpy)]^-/2e^-$ pathway (Figure S3).[22] These observations are consistent with the disruption of hydrogen-bonding; no cooperative bimetallic effect is observed under these conditions. Studies at low concentrations (0.2 mM and 0.5 mM) show the bimolecular pathway persists for **1** in MeCN and is also disrupted by solvation in *N*,*N*-DMF (Figures S4−S12). On the basis of this initial electrochemical survey, we focused on understanding the role of the Tyr side chain during catalysis

Isolating the Role of the Tyr Side Chain Electrochemically. In order to probe whether the phenolic residues of Tyr play a role in the observed catalytic response, a series of control experiments were conducted with **2**, which contains no −OH group. Under Ar saturation conditions in MeCN, **2** showed a similar redox response to **1** with four reduction features (irreversible: −1.78, −1.94, −2.27, and −2.50 V vs Fc/Fc+; Figure S13) that persisted at high scan rates (Figure S14). Under CO_2 saturation conditions, however, the observed current response was greatly diminished in comparison with **1** (maximum theoretical TOF = 0.92 s^{-1}; Figure 3). Only with added PhOH (0.5 M) does the catalytic response of **2** approach that observed for **1** (maximum theoretical TOF with 0.5 M PhOH = 56 s^{-1}; bulk electrolysis under CO_2 saturation with 0.5 M PhOH at −2.2 V vs Fc/Fc+ shows current efficiency for CO = 99%, H_2 = 0.12%). The difference in the observed potential for the first two redox features was less than that observed for **1**, corresponding to K_c = 347. Likewise, repeating these experiments in *N*,*N*-DMF indicated that the hydrogen-bonding effect responsible for the supramolecular dimer could be interrupted with the catalyst reverting to a unimolecular response (Figure S15).

Repeating these experiments for **1** and **2** using the bulky proton source 2,6-diisopropylphenol, dipPhOH, as a substitute for PhOH supports the hypothesis that the difference in the observed catalytic response between **1** and **2** is due to the Tyr

DOI: 10.1021/jacs.6b03774
J. Am. Chem. Soc. 2016, 138, 8184−8193

Scheme 3. Proposed Bimolecular Mechanism for the Reduction of CO_2 to CO and CO_3^{2-} by Complexes of the Type $Re^0(bpy)(CO)_3$ - Adapted from ref 22.

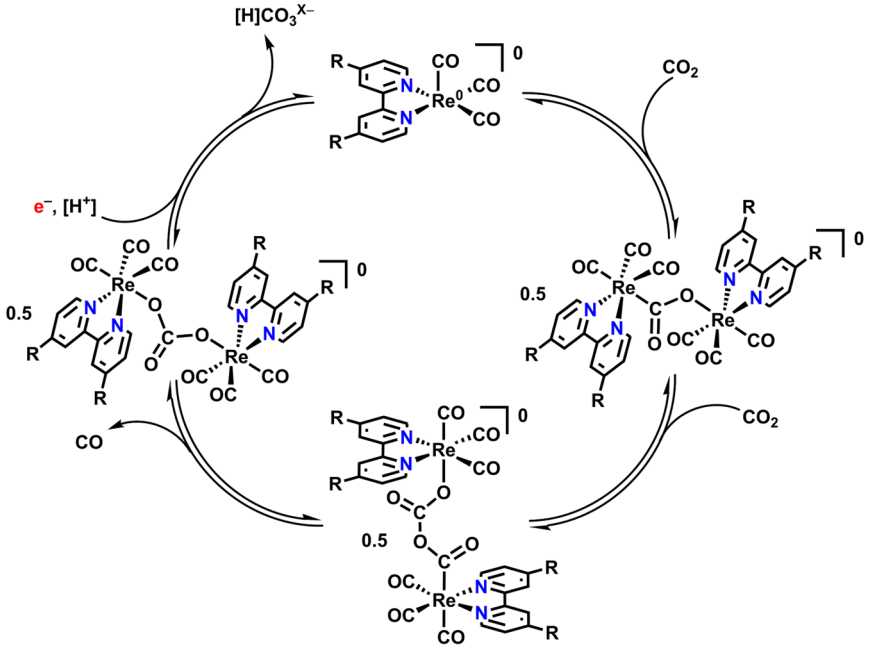

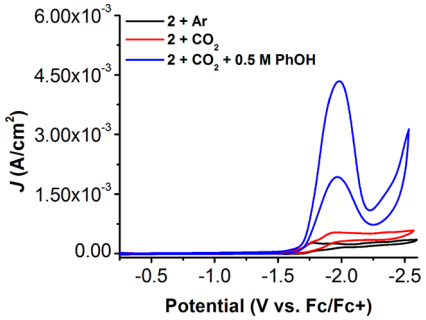

Figure 3. CVs of the current response of Re(**Phedac**)$(CO)_3$Cl (**2**) at negative potentials under Ar saturation conditions (black), CO_2 saturation (red), and CO_2 saturation with added PhOH (0.5 M; blue). Conditions: 1 mM in 0.1 $TBAPF_6$/MeCN; glassy carbon working electrode, Pt wire counter electrode, Ag/AgCl pseudoreference electrode; referenced to internal Fc standard; scan rate 100 mV/s.

residues acting as proton relays during catalysis. Compared to PhOH, dipPhOH has significant steric hindrance, such that intermolecular protonation rates from exogenous Brønsted acid should be kinetically slow. If the rate of intra/intermolecular protonation involving the Tyr residues is fast relative to exogenous protonation by dipPhOH, the difference between Phe and Tyr observed under CO_2 saturation only should be partially retained. Experimental observations show that excess dipPhOH (0.54 M) does indeed contribute to slower rates of catalysis when compared to near equimolar amounts of PhOH (Figure 4). Interestingly, the increase in current density arising from the addition of 0.54 M dipPhOH is almost identical for **1** and **2**, although **1** passes ~2.3 times more current than **2**. This is in contrast to PhOH, where the increase was much greater for **2** than for **1** (**1** passes ~1.3× current of **2** with 0.5 M PhOH, Figure 4). The persistent difference in current density between **1** and **2** under CO_2 saturation with dipPhOH is an indicator that Tyr is acting as an intramolecular proton relay to the metal centers during catalysis. On the basis of this hypothesis we elected to explore the dimer structures further by computational methods.

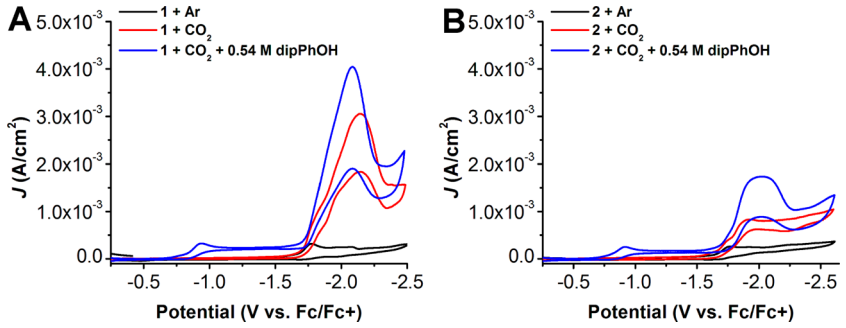

Figure 4. CVs of the current response of Re(**Tyrdac**)$(CO)_3$Cl (**1**) and Re(**Phedac**)$(CO)_3$Cl (**2**) at negative potentials under Ar saturation conditions (black), CO_2 saturation (red), and CO_2 saturation with added dipPhOH (0.54 M; blue). Conditions: 1 mM in 0.1 $TBAPF_6$/MeCN; glassy carbon working electrode, Pt wire counter electrode, Ag/AgCl pseudoreference electrode; referenced to internal Fc standard; scan rate 100 mV/s.

DOI: 10.1021/jacs.6b03774
J. Am. Chem. Soc. 2016, 138, 8184–8193

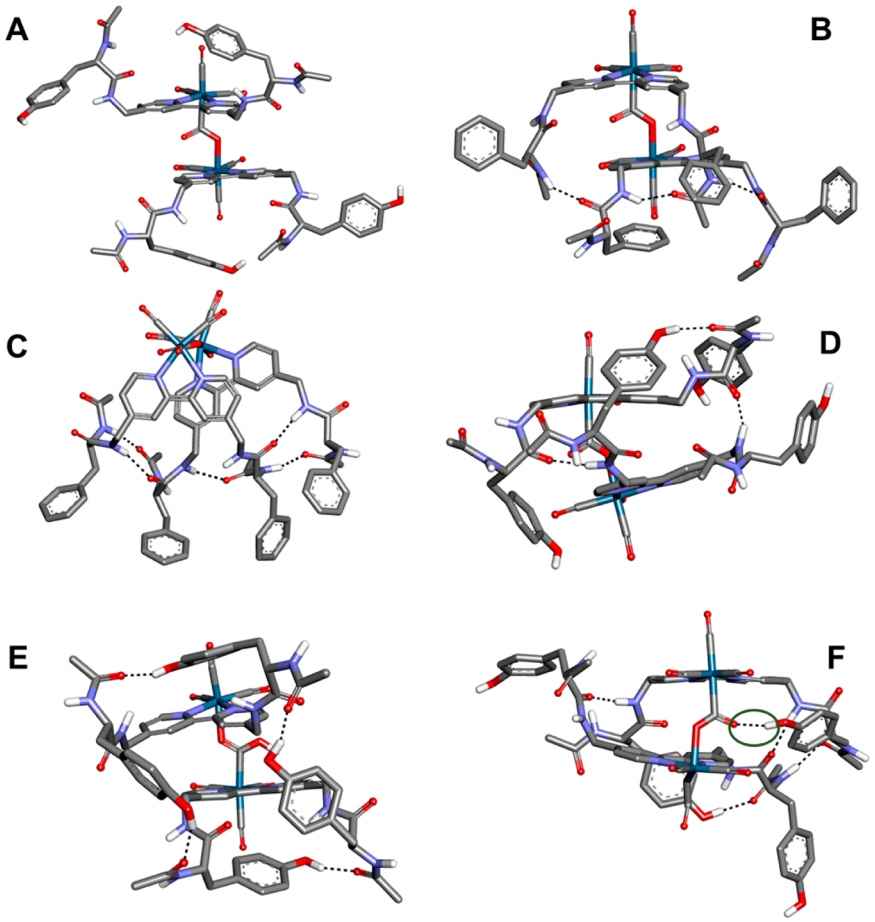

Figure 5. (A) The starting structure of [Re(**Tyrdac**)$(CO)_3]_2(\mu_2$-η^2-$CO_2)$ in the present simulations. Carbon: gray; oxygen: red; nitrogen: blue; rhenium: cyan; only polar hydrogen atoms are shown for clarity. [Re(**Phedac**)$(CO)_3]_2(\mu_2$-η^2-$CO_2)$ has a similar starting configuration (Figure S16) except that the four hydroxyl groups are replaced with hydrogen atoms. (B) Representative structure of the bridging μ_2-η^2-CO_2 adduct of **2**, [Re(**Phedac**)$(CO)_3]_2(\mu_2$-η^2-$CO_2)$. Dashed black lines indicate the hydrogen bonding interactions. (C) A snapshot from MD trajectory of [Re(**Phedac**)$(CO)_3]_2(\mu_2$-η^2-$CO_2)$, showing five hydrogen bonds. (D) [Re(**Tyrdac**)$(CO)_3]_2(\mu_2$-η^2-$CO_2)$ dimer formed via hydrogen bonding interactions between amide-amide and amide-phenol groups. (E) Phenol groups participate in both inter- and intramolecular interactions in [Re(**Tyrdac**)$(CO)_3]_2(\mu_2$-η^2-$CO_2)$. (F) A snapshot from MD trajectory of [Re(**Tyrdac**)$(CO)_3]_2(\mu_2$-η^2-$CO_2)$. The hydrogen bond between the bound CO_2 and the hydroxyl group in tyrosine residue is highlighted within the green circle; computational details are found in the Experimental Section below.

Simulations of Catalyst Behavior in Solution. Microsecond time scale molecular dynamics (MD) simulations with explicit MeCN were employed to explore the behavior of **1** and **2** in greater detail. In order to focus on catalytically relevant dimer structures in the available simulation time, we applied conformational restraints to model one molecule of CO_2 bound between two molecules of [Re(**Tyrdac**)$(CO)_3$] or [Re(**Phedac**)$(CO)_3$], with a cofacial alignment of the bipyridine ligands (Figure 5). Consistent with previous MD simulations of [Re(**dac**)$(CO)_3$],[22] hydrogen bonded dimers were observed in simulations beginning with stacked configurations of both [Re(**Tyrdac**)$(CO)_3]_2(\mu_2$-η^2-$CO_2)$ and [Re(**Phedac**)$(CO)_3]_2(\mu_2$-η^2-$CO_2)$ with the added restraints.[45] In the case of the [Re(**Phedac**)$(CO)_3]_2(\mu_2$-η^2-$CO_2)$ dimer, the most populated conformation contains three intermolecular hydrogen bonds, linking the amide moieties of the phenylalanine substituents (Figure 5B). However, due to the increased number of hydrogen bond donor and acceptor moieties compared to [Re(**dac**)$(CO)_3$], this system is capable of forming a wider variety of hydrogen-bonded conformations, with some containing four or even five hydrogen bonds in these simulations (Figure 5C).

Furthermore, the additional hydroxyl groups in the [Re(**Tyrdac**) $(CO)_3]_2(\mu_2$-η^2-$CO_2)$ dimer, versus the [Re(**Phedac**) $(CO)_3]_2(\mu_2$-η^2-$CO_2)$ dimer, allows it to form an even richer variety of hydrogen bonding patterns in the simulations. In particular, this Tyr-based dimer was observed to interconvert among configurations with hydrogen bond interactions involving not only the amide NH and CO groups, but also the OH groups of the tyrosine residues (Figure S16). Importantly, the OH groups of the tyrosine residues were observed to donate hydrogen bonds to the bound CO_2 during much of the simulation (Figure 5D). This means that the tyrosine phenol is capable of reaching the bridging μ_2-η^2-CO_2 molecule and is thus available to serve as a pendant, intramolecular proton source for the catalytic reaction. The accessibility of such configurations is consistent with the experimentally observed increase in activity under catalytic conditions for the tyrosine derivative, **1**, in comparison to the phenylalanine derivative, **2**, which of course lacks a phenol group.

Understanding Behavior Under Applied Potential with IR-Spectroelectrochemistry. Infrared spectroelectrochemistry (IR-SEC) is a powerful technique that has been used

DOI: 10.1021/jacs.6b03774
J. Am. Chem. Soc. 2016, 138, 8184−8193

previously for studying carbonyl-containing CO_2 reduction electrocatalysts.[22,46−51] With IR-SEC, a microscale electrolysis experiment allows changes in the IR spectrum to be characterized as a function of time and potential (Figure 6).

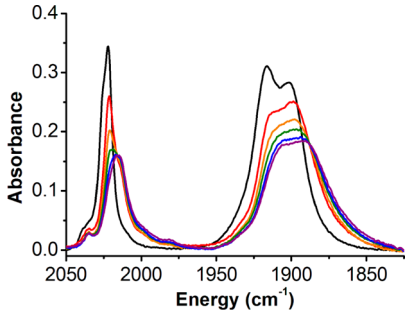

Figure 6. IR-SEC spectra of Re(**Tyrdac**)$(CO)_3$Cl (**1**) taken sequentially after the application of ∼−1.7 V vs Fc/Fc+ under N_2 saturation. At the first reduction potential observed by CV, the parent species **1** (black) rapidly equilibrates (∼5 minutes) to a species not previously observed for $[Re(bpy)(CO)_3(X)_m]^{n+}$ species during IR-SEC. The broadening of the individual features, as well as the fact that the metal-metal dimer $[Re(\textbf{Tyrdac})(CO)_3]_2$ is not observed until more negative potentials is suggestive of a transient mixed-valent state. Conditions: glassy carbon working electrode, Ag pseudoreference electrode, Pt counter electrode, 0.1 M $TBAPF_6$/MeCN, 4.7 mM **1**.

The resultant IR spectra can be correlated with other electrochemical techniques, like cyclic voltammograms, to build a comprehensive picture of electrochemical behavior in situ. Under N_2 atmosphere at resting potential, complex **1** was observed to have an IR signature consistent a *fac*-tricarbonyl Re(I) complex with bands at 2022, 1917, 1902 cm^{-1} (Figure 6). When the applied potential of the cell is increased negatively in a stepwise manner to that of the first reduction (∼ −1.7 V vs Fc/Fc+), these bands decreased in intensity with the concomitant appearance of a new tricarbonyl species with bands at 2017, 1904, and 1893 cm^{-1}. The shift and broadening of the IR features is not consistent with a single-electron reduction product — a unimolecular species which typically exhibits bands ∼15−20 wavenumbers lower in energy ($[Re(bpy)(CO)_3Cl]^-$ 1998, 1885, and 1867 cm^{-1}; $[Re(4,4'$-di-*tert*-butyl-2,2′-bipyridyl$)(CO)_3Cl]^-$ 2005, 1895, and 1878 cm^{-1})[7,48,51−53] — and indicates the formation of a new species on the IR-SEC time scale. This new species is stable until a more negative potential is reached (∼ −1.8 V vs Fc/Fc+), whereupon the formation of the metal−metal bonded dimer $[Re(\textbf{Tyrdac})(CO)_3]_2$ begins to occur. We have previously proposed that the splitting observed by cyclic voltammetry is consistent with a mixed-valent state,[22] and given the increased stability (as estimated by the comproportionation constant K_c) observed for **1**, it is likely that this new species represents a mixed-valent dimer, $([Re^{I}(\textbf{Tyrdac})(CO)_3][Re^{0}(\textbf{Tyrdac})(CO)_3])$.

Analogous IR-SEC experiments were undertaken with **2** (Figure S17), which indicated that although the mixed-valent state showed some stability on the IR-SEC time scale, the mixed-valent state of **2** is not as stable as that of **1**. Similar to the behavior observed for **1**, when the cell is charged with **2** and set to the potential of the first reduction (∼ −1.7 V vs Fc/Fc+), the parent stretches at 2022, 1915, 1899 cm^{-1} diminish in intensity with the concomitant appearance of a set of new bands. A species similar to the proposed mixed-valent state observed for **1** appears at 2018, 1905, and 1892 cm^{-1}, along with at least two additional species. The high frequency stretching modes observed at 2009 and 1996 cm^{-1} allow these species to be assigned to $[Re(\textbf{Phedac})(CO)_3Cl]^-$ and $[Re^{0}(\textbf{Phedac})(CO)_3]$, respectively.[52] Shifting the applied potential more negative than ∼ −1.7 V vs Fc/Fc+ results in the formation of a metal−metal dimer, $[Re(\textbf{Phedac})(CO)_3]_2$. These observations are consistent with the smaller K_c values determined for **2** experimentally, vide supra.

In order to experimentally confirm that a reductive disproportionation reaction was occurring, this experiment was repeated for **1** at the first reduction potential (∼ −1.7 V vs Fc/Fc+) with partial CO_2 saturation (Figure 7; see

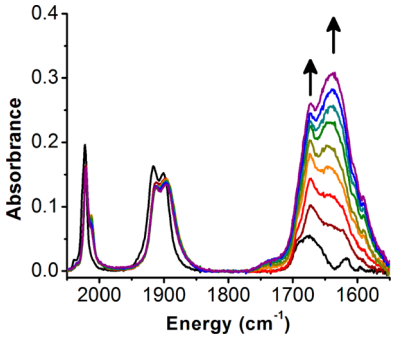

Figure 7. IR-SEC spectra of Re(**Tyrdac**)$(CO)_3$Cl (**1**) taken sequentially after the application of ∼ −1.7 V vs Fc/Fc+ under partial CO_2 saturation. At the first reduction potential observed by CV for **1**, bands consistent with the formation of carbonate at 1639 and 1672 cm^{-1} appear and increase in intensity over the course of 20 min (2 min time points). Free CO is also observed (Figure S18). Conditions: glassy carbon working electrode, Ag pseudoreference electrode, Pt counter electrode, 0.1 M $TBAPF_6$/MeCN, 4.0 mM **1**.

Experimental Section). Consistent with a reductive disproportionation mechanism, two IR bands diagnostic of CO_3^{2-} at 1639 and 1672 cm^{-1} are observed to increase in intensity over the course of the experiment (20 min);[22,54] free CO appears at 2138 cm^{-1} (Figures S18 and S19).[22]

DISCUSSION AND CONCLUSIONS

The experimental results detailed above confirm that the expansion of our previously reported Re(**dac**)$(CO)_3$Cl ligand platform with single amino acid residues can enhance the selectivity and activity of the bimolecular active state. This can be attributed to the stabilization of the bimolecular active species through an increased number of hydrogen bond donors and acceptors and the inclusion of pendant proton sources. Indeed, a series of 2D NMR experiments on **1** showed that prior to reduction, a stable conformation of the peptide arms exists in solution on the NMR time scale. Specifically, the combination of rotating frame Overhauser effect spectroscopy (ROESY) in conjunction with total correlated spectroscopy (TOCSY) enabled the isolation of purely through-space interactions. These experiments revealed that the methylene protons and the side chain stereocenters of **1** had stable conformations relative to each other and to the bipyridine ligand (Figure S20, validated with TOCSY Figure S21). Comparable experiments on **2** revealed that on the NMR time scale such interactions were not relevant (Figure S22, validated with TOCSY Figure S23). These data are consistent with the respective K_c values for these two compounds, which

DOI: 10.1021/jacs.6b03774
J. Am. Chem. Soc. 2016, 138, 8184−8193

show that **1** exhibits stronger mixed-valence coupling than **2**. In order for there to be a stable mixed-valent state in these compounds, there must be a pre-equilibrium involving hydrogen bonding prior to the application of potential. On the basis of this and the observed K_c values, it is likely that the conformation **1** adopts in solution prior to reduction has a greater relevance to the conformation of the mixed-valent state. The N*H* ^{1}H NMR resonances of **1** exhibited a concentration dependence, however, this was not found to be an accurate diagnostic indicator of the bimolecular hydrogen bonding, likely due to competing intraligand interactions (Figures S24 and S25).

These data also suggest that the acylated tyrosine residue plays an important role in the process of supramolecular assembly. Since tyrosine can be a hydrogen bond donor or acceptor in the protonated form, and an acceptor when deprotonated, it is likely that the additional stabilization of the mixed-valent state observed for **1** is the result of tyrosine participation in hydrogen-bonding interactions. MD simulations support this idea, as they reveal various conformations with noncovalent inter- and intramolecular interactions that involve the phenol group. In addition to this, the difference in catalytic activity between **1** and **2** supports the notion that these residues can also act as a pendant proton source. In the absence of external Brønsted acid, the i_{cat}/i_p values, which approximate relative catalytic rates on the CV time scale, give values 7.7× higher for **1** than for **2**. This effect diminishes in the presence of an excess of external proton source (0.5 M PhOH), with both catalysts achieving similar current densities. This suggests that **2** adopts a suitable bimolecular conformation for catalysis at applied potential but is limited by the absence of Brønsted acid. Further evidence of this is seen in the data taken with dipPhOH, which has greater steric bulk than PhOH and is thus expected to contribute protons at a kinetically limited rate. Indeed, both catalysts show an increase in current under catalytic conditions for CO_2 reduction with 0.54 M dipPhOH; however, **1** achieves more than double the current density of **2**, which would be expected if the rate of protonation by the tyrosine residues was relevant under these conditions.

The incorporation of additional amino acid residues at the 4 and 4′ positions on the bipyridine not only preserves the previously reported bimolecular catalytic mechanism, it also expands the pool of ligand modifications to include pendant proton sources. In a manner independent of traditional steric or electronic modifications, this system shifts to an entirely bimolecular catalytic mechanism while preserving the efficiency of the unimolecular process at less negative potentials. These results are promising for understanding how active sites assembled by noncovalent means can be tailored to improve catalytic activity and efficiency. In order to improve the observed activity, we have begun exploring the inclusion of additional abiotic and biotic amino acid residues to expand the pool of cocatalytic moieties for this system. Given the general interest in lowering electrocatalyst operating potentials for a variety of transformations, the use of noncovalent assembly methods is intriguing for future studies of other catalyst systems as well.

EXPERIMENTAL SECTION

General Methods. ^{1}H NMR and ^{13}C{^{1}H} spectra were recorded on a 500 MHz Varian spectrometer at 298 K and referenced to residual solvent shifts. Data manipulations were completed using ACD or iNMR. Infrared spectra were taken on a Thermo Scientific Nicolet 6700 or a Bruker Equinox 55 spectrometer. Microanalyses were performed by Midwest Microlab for C, H, and N. ESI-MS data were taken at the UCSD Molecular Mass Spectrometry Facility.

Solvents and Chemicals. All solvents were obtained from Fisher Scientific. All solvents were dried in house by storing in a moisture free environment and dried on a custom drying system running through two alumina columns prior to use. All compounds were obtained from Fisher Scientific or Sigma-Aldrich and used as obtained unless otherwise specified. Tetrabutylammonium hexafluorophosphate ($TBAPF_6$, Aldrich, 98%) was recrystallized from CH_3OH and dried at 90 °C overnight under a vacuum before use in electrochemistry. 4,4′-bis(methylamine)-2,2′-bipyridine was prepared according to a literature procedure.[22,55]

Synthetic Methods. *General Procedure of NHS-Ester Coupling.* In a round-bottom flask the FMOC-protected ester, 1.1 equiv *N*-hydroxysuccinimide, 1.1 equiv *N*,*N*-diisopropyl carbodiimide, and 1.1 equiv triphenylamine were suspended in CH_2Cl_2 and stirred for 1 h. After this time, 0.5 equiv of 4,4′-bis(methylamine)-2,2′-bipyridine were added and the reaction stirred for an additional 2 h. Purification was accomplished by filtration and washing with minimal CH_2Cl_2 (2 × 5 mL).

4,4′-Bis(methylamido-Tyr(tBu)-N-FMOC)-2,2′-bipyridyl, ***b***. Yield (isolated) 2.5 g, 98%. ^{1}H NMR (*N*,*N*-DMF-d_7, 400 MHz): δ 8.77 (m, 2H, ArH), 8.59 (m, 2H, ArH), 8.42 (s, 2H, ArH), 7.93 (d, 2H, ArH), 7.73 (m, 2H, ArH), 7.44 (m, 2H, ArH), 7.33 (m, 4H, ArH), 7.07 (m, 4H, ArH), 6.89 (d, 2H, ArH), 5.56 (br m, 4H, $-CH_2NHC(O)R$), 4.55 (m, 6H, $-CH_2-$), 4.19 (m, 6H, $-CH_2-$), 3.22 (m, 2H, $-CH(CH_2-)-$), 2.99 (m, 2H, $-CH(CH_2-)-$), 1.23 (br s, 18H, $-CH_3$). Elemental Analysis for $C_{68}H_{68}N_6O_8\cdot0.5CH_2Cl_2$ Calc'd: C 72.18, H 6.10, N 7.37; Found: C 71.30, H 6.35, N 8.70. ESI-MS (*m*/*z*) $[M + H]^+$: Calc'd 1097.52. Found: 1097.74.

4,4′-Bis(methylamido-Phe-N-FMOC)-2,2′-bipyridyl, ***e***. Yield (isolated) 1.94 g, 87%. ^{1}H NMR (*N*,*N*-DMF-d_7, 400 MHz): δ 8.78 (m, 2H, ArH), 8.56 (m, 2H, ArH), 8.40 (s, 2H, ArH), 8.03 (m, 2H, ArH), 7.92 (m, 2H, ArH), 7.77 (m, 2H, ArH), 7.70 (m, 2H, ArH), 7.41 (m, 6H, ArH), 7.29 (m, 8H, ArH), 7.21 (m, 2H, ArH), 7.05 (d, 2H, ArH), 5.56 (br m, 4H, $-CH_2NHC(O)R$), 4.55 (m, 6H, $-CH_2-$), 4.21 (m, 6H, $-CH_2-$), 3.26 (m, 2H, $-CH(CH_2-)-$), 3.05 (m, 2H, $-CH(CH_2-)-$). Elemental Analysis for $C_{60}H_{52}N_6O_6\cdot C_4H_5NO_3\cdot C_7H_{16}N_2O$ Calc'd: C 70.34, H 6.07, N 10.40; Found: C 69.00, H 5.72, N 10.34. ESI-MS (*m*/*z*) $[M+Na+H^+]^{2+}$: Calc'd 488.20. Found: 489.42.

General Procedure for FMOC Deprotection and Acetylation. In a round-bottom flask the FMOC-protected ligand and 2.1 equiv 4-methylpiperidine were suspended in CH_2Cl_2 and stirred for 1 h. After this time, 2.1 equiv of Et_3N and 2.1 equiv of acetic anhydride were added and the reaction stirred for an additional 2 h. Purification was accomplished by removing all solvent under reduced pressure, suspending in CH_2Cl_2 and filtering, followed by washing with Et_2O (2 × 10 mL).

4,4′-Bis(methylamido-Tyr(tBu)-N-acyl)-2,2′-bipyridyl, ***c, Tyrdac-tBu***. Yield (isolated) 0.42 g, 42%. ^{1}H NMR (*N*,*N*-DMF-d_7, 400 MHz): δ 8.61 (m, 2H, ArH), 8.39 (m, 2H, ArH), 8.16 (s, 2H, ArH), 7.24 (d, 4H, ArH), 6.91 (m, 4H, ArH), 5.56 (br m, 4H, $-CH_2NHC(O)R$), 4.70 (m, 2H, $-CH(CH_2-)-$), 4.50 (m, 4H, $-CH_2-$), 3.15 (m, 4H, $-CH_2-$), 1.89 (br s, 6H, $-CH_3$), 1.23 (br s, 18H, $-CH_3$). Elemental Analysis for $C_{42}H_{52}N_6O_6$ Calc'd: C 68.46, H 7.11, N 11.40; Found: C 68.76, H 6.86, N 10.06. ESI-MS (*m*/*z*) $[M+H]^+$: Calc'd 737.40. Found: 737.42.

4,4′-Bis(methylamido-Phe-N-acyl), ***f, Phedac***. Yield (isolated) 0.47 g, 76%. ^{1}H NMR (*N*,*N*-DMF-d_7, 400 MHz): δ 8.61 (m, 2H, ArH), 8.38 (m, 2H, ArH), 8.20 (s, 2H, ArH), 7.29 (m, 10H, ArH), 5.56 (br m, 4H, $-CH_2NHC(O)R$), 4.73 (m, 2H, $-CH(CH_2-)-$), 4.51 (m, 4H, $-CH_2-$), 3.17 (m, 4H, $-CH_2-$3.15 (m, 4H, $-CH_2-$), 1.89 (br s, 6H, $-CH_3$). Elemental Analysis for $C_{34}H_{36}N_6O_6\cdot0.5CH_2Cl_2$ Calc'd: C 65.24, H 5.87, N 13.23; Found: C 65.69, H 6.25, N 12.25. ESI-MS (*m*/*z*) $[M + H]^+$: Calc'd 593.29. Found: 593.56.

Re(Tyrdac)(CO)$_3$Cl. A round-bottom flask was charged with **Tyrdac** (0.250 g, 0.34 mmol) and $Re(CO)_5Cl$ (0.123 g, 0.34 mmol) in dry, degassed toluene (20 mL). The mixture was heated to reflux

DOI: 10.1021/jacs.6b03774
J. Am. Chem. Soc. 2016, 138, 8184−8193

under N_2 atmosphere and stirred at reflux for 3 h. After this time the solution was allowed to cool to room temperature, before being condensed under reduced pressure. The resulting yellow solid was dissolved in a mixture of dichloromethane and trifluoroacetic acid (5:95, 5 mL) and stirred for 1 h before an excess of Et_2O was added to induce precipitation of a yellow powder. This yellow powder was filtered from the supernatant and washed with additional Et_2O (2 × 20 mL). Yield (isolated) 0.265 g, 84%. ^{1}H NMR (*N*,*N*-DMF-d_7, 500 MHz): δ 9.39 (br s, 2H, ArO*H*), 8.99 (sh d, 2H, Ar*H*), 8.81 (sh s, 2H, Ar*H*), 8.73 (br d, 2H, Ar*H*), 8.29 (br s, 2H, −CHN*H*CO(CH$_3$)), 7.57 (br dd, 2H, −CH$_2$N*H*COCH−), 7.13 (sh d, 4H, Ar*H*), 6.77 (br d, 4H, Ar*H*), 4.73 (br, diastereotopic 4H, −C−C*H*$_2$−NH−), 4.57 (br t, 2H, −ArC−C*H*−NH−), 3.50 (br s, (*H*$_2$O) 3.09 (br, diastereotopic 4H, −ArC−C*H*$_2$−CH−), 1.95 (sh s, 6H, −C*H*$_3$). ^{13}C{^{1}H} NMR (*N*,*N*-DMF-d_7, 500 MHz): δ 198.8 (2C, *C*≡O), 190.9 (1C, axial *C*≡O), 173.1 (2C, −NH−*C*O−CH), 171.1 (2C, −NH−*C*O−CH$_3$), 157.2 (2C, ArC−OH), 156.3 (2C, Ar*C*−CH$_2$), 155.1 (2C, ArC−ArC), 153.2 (2C, ArCH−ArCH−ArN), 130.8 (4C, Ar*C*H), 128.9 (2C, Ar*C*), 126.1 (2C, Ar*C*H), 122.9 (2C, Ar*C*H), 115.8 (4C, Ar*C*H), 56.7 (2C, *C*H), 42.2 (2C, ArC−CH$_2$−NH−), 37.4 (2C, −ArC−*C*H$_2$−CH−), 22.7 (2C, −CH$_3$). Elemental Analysis for $C_{37}H_{36}ClN_6O_9Re{\cdot}0.66CH_2Cl_2$ Calc'd: C 45.86, H 3.81, N 8.52; Found: C 45.82, H 4.21, N 7.96. ESI-MS (*m*/*z*) [M−Cl]$^+$: Calc'd 895.21. Found: 895.41. IR (MeCN) ν_{CO}: 2022, 1917, 1902 cm^{-1}.

Re(Phedac)(CO)$_3$Cl, 2. A round-bottom flask was charged with **Phedac** (0.125 g, 0.21 mmol) and Re(CO)$_5$Cl (0.076 g, 0.21 mmol) in dry, degassed Toluene (50 mL). The mixture was heated to reflux under N_2 atmosphere and stirred at reflux for 18 h. After this time the solution was allowed to cool to room temperature and placed in the freezer for 1h at −20 °C. The resulting yellow solid was separated from the supernatant by filtration and recrystallized from CH_2Cl_2 with pentanes. Yield (isolated) 0.134 g, 71%. ^{1}H NMR (*N*,*N*-DMF-d_7, 500 MHz): δ 8.98 (sh d, 2H, Ar*H*), 8.78 (sh d, 2H, Ar*H*), 8.58 (br dd, 2H, −CHN*H*CO(CH$_3$)), 8.36 (sh s, 2H, Ar*H*), 7.72 (sh dd, 2H, −CH$_2$N*H*COCH−), 7.30 (sh mult, 10H, Ar*H*), 4.71 (br mult, 2H, −CH$_2$−C*H*−NH−), 4.63 (br, diastereotopic 4H, −ArC−C*H*$_2$−CH−), 3.50 (br s, (*H*$_2$O), 1.88 (br, diastereotopic 4H, −CO−C*H*$_2$−NH−), 0.87 (sh s, 6H, −C*H*$_3$). ^{13}C{^{1}H} NMR (*N*,*N*-DMF-d_7, 500 MHz): δ 198.9 (2C, *C*≡O), 190.7 (1C, axial *C*≡O), 172.6 (2C, −NH−*C*O−CH$_3$), 171.0 (2C, −NH−*C*O−CH), 156.4 (2C, ArC−ArC), 154.8 (2C, Ar*C*−CH$_2$), 153.2 (2C, ArCH−ArCH−ArN), 138.9 (2C, Ar*C*), 129.9 (4C, Ar*C*H), 128.9 (4C, Ar*C*H), 127.8 (2C, Ar*C*H), 119.5 (2C, Ar*C*H), 116.0 (2C, Ar*C*H), 56.3 (2C, *C*H), 42.2 (2C, −ArC−CH$_2$−NH−), 38.1 (2C, −ArC−*C*H$_2$−CH−), 22.8 (2C, −CH$_3$). Elemental Analysis for $C_{37}H_{36}ClN_6O_7Re{\cdot}0.5\ CH_2Cl_2{\cdot}0.25\ C_5H_{12}$ Calc'd: C 47.87, H 3.96, N 8.93; Found: C 45.97, H 3.71, N 9.21. ESI-MS (*m*/*z*) [M−Cl]$^+$: Calc'd 863.22. Found: 863.23. IR (MeCN) ν_{CO}: 2022, 1915, 1899 cm^{-1}.

Cyclic Voltammetry. Electrochemical experiments were carried out using a BASi Epsilon potentiostat. For all experiments, a single compartment cell was used with dry stir bar and a dry needle was connected to control the atmosphere. A 3 mm diameter glassy carbon electrode from BASi was employed as the working electrode. The counter electrode was a platinum wire and the reference electrode was a silver/silver chloride electrode separated from solution by a CoralPor tip. Experiments were run with and without an added internal reference of ferrocene. All solutions were in dry acetonitrile and contained 1 mM of **1** and 0.1 M tetrabutylammonium hexafluorophosphate ($TBAPF_6$) as the supporting electrolyte. Experiments were purged with Ar or CO_2 (to saturation at 0.28 M) before CVs were taken and stirred in between successive experiments. All experiments were reported referenced an internal ferrocene standard except for the bulk electrolysis experiments which used the pseudoreference Ag/AgCl behind a CoralPor tip.

Infrared Spectroelectrochemistry. The experimental setup and design of the IR-SEC cell has been published previously by our lab.[50,52] A Pine Instrument Company model AFCBP1 bipotentiostat was employed. As the potential was scanned, thin layer bulk electrolysis was monitored by Fourier-Transform Reflectance IR off the electrode surface. All experiments were conducted in 0.1 M $TBAPF_6$/MeCN solutions with catalyst concentrations of ∼5 mM (unless otherwise noted) prepared under a nitrogen atmosphere. The IR-SEC cells used (working electrode/counter electrode/pseudoreference electrode) were either glassy carbon/Ag/Pt or Pt/Ag/Pt, meaning that all potentials were in reference to a pseudoreference redox couple, Ag/Ag+ (∼+200 mV from the Fc/Fc+ couple). For all experiments under catalytic conditions the samples were sparged with CO_2 for 10 s.

Bulk Electrolysis. Bulk electrolyses were performed in a custom threaded glass jar from Chemglass fitted with a custom PEEK top containing ports for venting, fritted glass insert with counter electrode, working electrode, counter electrode, and a septum for sampling the headspace. The system was sealed with a combination of o-rings, Teflon tape, and electrical tape and tested for airtightness before each run. For an individual run the jar was charged with a known amount of catalyst (around 1 mM in 40 mL of solvent), known amount of PhOH (0.5 M), stir bar, and an electrolyte solution (0.1 M $TBAPF_6$/MeCN) before being sparged to saturation with CO_2. In order to prevent polymerization of PhOH on the counter electrode, 0.1 M Fc was added to the electrolyte solution as a sacrificial oxidant. After a run was completed, the headspace was sampled via airtight syringe and characterized by GC such that Faradaic efficiency could be determined by using a calibration curve.

Computational Methods. MD simulations were performed with the package Gromacs 5.0[56] at 298.15 K, with explicit MeCN solvent. The starting structures were built based on the DFT optimized structure of [Re(**dac**)(CO)$_3$]$_2$(μ_2-η^2-CO$_2$) from our previous study,[22] with tyrosine or phenylalanine residues added to the methyl acetamidomethyl substituents. To reduce bias introduced by the initial configuration, substituents were rotated in a way to diminish interactions between two monomers. Restraints were put on the bonds, angles and torsions that involve the two rhenium atoms as well as the bridging μ_2-η^2-CO$_2$ molecule during the entire simulation time to prevent two monomers from drafting apart. The Lennard−Jones parameters of rhenium in the octahedral configuration were obtained from the universal force field.[57] The rest of the bonded and van der Waals parameters in the system were obtained from the general Amber force field (GAFF), except that the torsion parameters of the amide bonds were modified according to the protein force field AMBER99-ILDN.[58] Partial atomic charges were derived by fitting the electrostatic potential generated through Gaussian 09[59] using the restrained electrostatic potential approach (RESP)[60] and Antechamber program.[61]

Each dimer species was solvated in a cubic box of acetonitrile with an edge length of 4.5 nm. Solute atoms were fixed at the initial coordinates using position restraints during the equilibration phase of added MeCN. After that, the position restraints were removed, but the bond, angle and torsion restraints involving rhenium and CO_2 were retained during the production phase. The production run lasted for 1 μs at constant temperature and pressure. The Particle Mesh Ewald method[62] was used to account for long-ranged electrostatic interactions, and the Lennard−Jones cutoff distance was set to 10 Å.

■ ASSOCIATED CONTENT

Supporting Information

The Supporting Information is available free of charge on the ACS Publications website at DOI: 10.1021/jacs.6b03774.

A selection of cyclic voltammograms, X-ray crystallographic information tables, and IR-SEC plots. (PDF)

Movie S1. A fragment (∼30 ns) of the microsecond-duration MD trajectory of [Re(**Phedac**)(CO)$_3$]$_2$(μ_2-η^2-CO$_2$) simulated in explicit MeCN. The system shows a strong preference for conformations with three intermolecular hydrogen bonds connecting the amide moieties of the amino acid substituents. Carbon: cyan; oxygen: red; nitrogen: blue; rhenium: pink. Hydrogen atoms are omitted for clarity. (MPG)

DOI: 10.1021/jacs.6b03774
J. Am. Chem. Soc. 2016, 138, 8184−8193

AUTHOR INFORMATION

Corresponding Author

*ckubiak@ucsd.edu

Notes

The authors declare the following competing financial interest(s): M.K.G. has an equity interest in, and is a cofounder and scientific advisor of VeraChem LLC.

ACKNOWLEDGMENTS

We acknowledge support for this work from the AFOSR through a Basic Research Initiative (BRI) grant (FA9550-12-1-0414) and the UCSD Department of Chemistry and Biochemistry for analytical instrumentation. S.A.C. thanks the NSF for support through a GFRP award.

REFERENCES

(1) Benson, E. E.; Kubiak, C. P.; Sathrum, A. J.; Smieja, J. M. *Chem. Soc. Rev.* **2009**, *38*, 89.
(2) Finn, C.; Schnittger, S.; Yellowlees, L. J.; Love, J. B. *Chem. Commun.* **2012**, *48*, 1392.
(3) Inglis, J. L.; MacLean, B. J.; Pryce, M. T.; Vos, J. G. *Coord. Chem. Rev.* **2012**, *256*, 2571.
(4) Costentin, C.; Robert, M.; Saveant, J.-M. *Chem. Soc. Rev.* **2013**, *42*, 2423.
(5) Qiao, J.; Liu, Y.; Hong, F.; Zhang, J. *Chem. Soc. Rev.* **2014**, *43*, 631.
(6) Hawecker, J.; Lehn, J.-M.; Ziessel, R. *J. Chem. Soc., Chem. Commun.* **1984**, 328.
(7) Smieja, J. M.; Kubiak, C. P. *Inorg. Chem.* **2010**, *49*, 9283.
(8) Benson, E. E.; Kubiak, C. P. *Chem. Commun.* **2012**, *48*, 7374.
(9) Smieja, J. M.; Benson, E. E.; Kumar, B.; Grice, K. A.; Seu, C. S.; Miller, A. J. M.; Mayer, J. M.; Kubiak, C. P. *Proc. Natl. Acad. Sci. U. S. A.* **2012**, *109*, 15646.
(10) Benson, E. E.; Grice, K. A.; Smieja, J. M.; Kubiak, C. P. *Polyhedron* **2013**, *58*, 229.
(11) Benson, E. E.; Sampson, M. D.; Grice, K. A.; Smieja, J. M.; Froehlich, J. D.; Friebel, D.; Keith, J. A.; Carter, E. A.; Nilsson, A.; Kubiak, C. P. *Angew. Chem., Int. Ed.* **2013**, *52*, 4841.
(12) Grice, K. A.; Gu, N. X.; Sampson, M. D.; Kubiak, C. P. *Dalton Trans.* **2013**, *42*, 8498.
(13) Keith, J. A.; Grice, K. A.; Kubiak, C. P.; Carter, E. A. *J. Am. Chem. Soc.* **2013**, *135*, 15823.
(14) Sampson, M. D.; Froehlich, J. D.; Smieja, J. M.; Benson, E. E.; Sharp, I. D.; Kubiak, C. P. *Energy Environ. Sci.* **2013**, *6*, 3748.
(15) Grice, K. A.; Kubiak, C. P. In *Adv. Inorg. Chem.*; Aresta, M., van Eldik, R., Eds.; Academic Press: San Diego, CA, 2014.
(16) Bourrez, M.; Molton, F.; Chardon-Noblat, S.; Deronzier, A. *Angew. Chem., Int. Ed.* **2011**, *50*, 9903.
(17) Sampson, M. D.; Nguyen, A. D.; Grice, K. A.; Moore, C. E.; Rheingold, A. L.; Kubiak, C. P. *J. Am. Chem. Soc.* **2014**, *136*, 5460.
(18) Smieja, J. M.; Sampson, M. D.; Grice, K. A.; Benson, E. E.; Froehlich, J. D.; Kubiak, C. P. *Inorg. Chem.* **2013**, *52*, 2484.
(19) Sullivan, B. P.; Bolinger, C. M.; Conrad, D.; Vining, W. J.; Meyer, T. J. *J. Chem. Soc., Chem. Commun.* **1985**, 1414.
(20) Hayashi, Y.; Kita, S.; Brunschwig, B. S.; Fujita, E. *J. Am. Chem. Soc.* **2003**, *125*, 11976.
(21) Agarwal, J.; Fujita, E.; Schaefer, H. F.; Muckerman, J. T. *J. Am. Chem. Soc.* **2012**, *134*, 5180.
(22) Machan, C. W.; Chabolla, S. A.; Yin, J.; Gilson, M. K.; Tezcan, F. A.; Kubiak, C. P. *J. Am. Chem. Soc.* **2014**, *136*, 14598.
(23) Dobbek, H.; Svetlitchnyi, V.; Gremer, L.; Huber, R.; Meyer, O. *Science* **2001**, *293*, 1281.
(24) Jeoung, J.-H.; Dobbek, H. *Science* **2007**, *318*, 1461.
(25) Kung, Y.; Drennan, C. L. *Curr. Opin. Chem. Biol.* **2011**, *15*, 276.
(26) Dutta, A.; Lense, S.; Hou, J.; Engelhard, M. H.; Roberts, J. A. S.; Shaw, W. J. *J. Am. Chem. Soc.* **2013**, *135*, 18490.
(27) Dutta, A.; Roberts, J. A. S.; Shaw, W. J. *Angew. Chem., Int. Ed.* **2014**, *53*, 6487.
(28) Ginovska-Pangovska, B.; Dutta, A.; Reback, M. L.; Linehan, J. C.; Shaw, W. J. *Acc. Chem. Res.* **2014**, *47*, 2621.
(29) Reback, M. L.; Ginovska-Pangovska, B.; Ho, M.-H.; Jain, A.; Squier, T. C.; Raugei, S.; Roberts, J. A. S.; Shaw, W. J. *Chem. - Eur. J.* **2013**, *19*, 1928.
(30) Galan, B. R.; Reback, M. L.; Jain, A.; Appel, A. M.; Shaw, W. J. *Eur. J. Inorg. Chem.* **2013**, *2013*, 5366.
(31) Severin, K.; Bergs, R.; Beck, W. *Angew. Chem., Int. Ed.* **1998**, *37*, 1634.
(32) Shaw, W. J. *Catal. Rev.: Sci. Eng.* **2012**, *54*, 489.
(33) Hoarau, M.; Hureau, C.; Gras, E.; Faller, P. *Coord. Chem. Rev.* **2016**, *308*, 445.
(34) Franco, F.; Cometto, C.; Ferrero Vallana, F.; Sordello, F.; Priola, E.; Minero, C.; Nervi, C.; Gobetto, R. *Chem. Commun.* **2014**, *50*, 14670.
(35) Agarwal, J.; Shaw, T. W.; Schaefer, H. F.; Bocarsly, A. B. *Inorg. Chem.* **2015**, *54*, 5285.
(36) Costentin, C.; Drouet, S.; Robert, M.; Savéant, J.-M. *Science* **2012**, *338*, 90.
(37) Costentin, C.; Passard, G.; Robert, M.; Savéant, J.-M. *Proc. Natl. Acad. Sci. U. S. A.* **2014**, *111*, 14990.
(38) Costentin, C.; Passard, G.; Robert, M.; Savéant, J.-M. *J. Am. Chem. Soc.* **2014**, *136*, 11821.
(39) Bagherzadeh, S.; Mankad, N. P. *J. Am. Chem. Soc.* **2015**, *137*, 10898.
(40) Mankad, N. P. *Chem. - Eur. J.* **2016**, *22*, 5822.
(41) Ito, T.; Hamaguchi, T.; Nagino, H.; Yamaguchi, T.; Kido, H.; Zavarine, I. S.; Richmond, T.; Washington, J.; Kubiak, C. P. *J. Am. Chem. Soc.* **1999**, *121*, 4625.
(42) Savéant, J. M.; Vianello, E. *Electrochim. Acta* **1963**, *8*, 905.
(43) Bard, A. J.; Faulkner, L. R. *Electrochemical Methods: Fundamentals and Applications*, 2nd ed.; John Wiley & Sons, Inc.: Hoboken, NJ, 2001.
(44) Machan, C. W.; Sampson, M. D.; Kubiak, C. P. *J. Am. Chem. Soc.* **2015**, *137*, 8564.
(45) Gibson, D. H. *Chem. Rev.* **1996**, *96*, 2063.
(46) Salsman, J. C.; Kubiak, C. P. In *Spectroelectrochemistry*; Kaim, W., Klein, A., Eds.; Royal Society of Chemistry: Cambridge, England, 2008.
(47) Ashley, K.; Pons, S. *Chem. Rev.* **1988**, *88*, 673.
(48) Christensen, P.; Hamnett, A.; Muir, A. V. G.; Timney, J. A. *J. Chem. Soc., Dalton Trans.* **1992**, 1455.
(49) Kaim, W.; Fiedler, J. *Chem. Soc. Rev.* **2009**, *38*, 3373.
(50) Zavarine, I. S.; Kubiak, C. P. *J. Electroanal. Chem.* **2001**, *495*, 106.
(51) Stor, G. J.; Hartl, F.; van Outersterp, J. W. M.; Stufkens, D. J. *Organometallics* **1995**, *14*, 1115.
(52) Machan, C. W.; Sampson, M. D.; Chabolla, S. A.; Dang, T.; Kubiak, C. P. *Organometallics* **2014**, *33*, 4550.
(53) Johnson, F. P. A.; George, M. W.; Hartl, F.; Turner, J. J. *Organometallics* **1996**, *15*, 3374.
(54) Simón-Manso, E.; Kubiak, C. P. *Organometallics* **2004**, *24*, 96.
(55) Beer, P. D.; Szemes, F.; Passaniti, P.; Maestri, M. *Inorg. Chem.* **2004**, *43*, 3965.
(56) Abraham, M. J.; Murtola, T.; Schulz, R.; Páll, S.; Smith, J. C.; Hess, B.; Lindahl, E. *SoftwareX* **2015**, *1−2*, 19.
(57) Wang, J.; Wolf, R. M.; Caldwell, J. W.; Kollman, P. A.; Case, D. A. *J. Comput. Chem.* **2004**, *25*, 1157.
(58) Lindorff-Larsen, K.; Piana, S.; Palmo, K.; Maragakis, P.; Klepeis, J. L.; Dror, R. O.; Shaw, D. E. *Proteins: Struct., Funct., Genet.* **2010**, *78*, 1950.
(59) Frisch, M. J.; Trucks, G. W.; Schlegel, H. B.; Scuseria, G. E.; Robb, M. A.; Cheeseman, J. R.; Scalmani, G.; Barone, V.; Mennucci, B.; Petersson, G. A.; Nakatsuji, H.; Caricato, M.; Li, X.; Hratchian, H. P.; Izmaylov, A. F.; Bloino, J.; Zheng, G.; Sonnenberg, J. L.; Hada, M.; Ehara, M.; Toyota, K.; Fukuda, R.; Hasegawa, J.; Ishida, M.; Nakajima, T.; Honda, Y.; Kitao, O.; Nakai, H.; Vreven, T.; Montgomery, J. A., Jr.;

DOI: 10.1021/jacs.6b03774
J. Am. Chem. Soc. 2016, 138, 8184−8193

Peralta, J. E.; Ogliaro, F.; Bearpark, M.; Heyd, J. J.; Brothers, E.; Kudin, K. N.; Staroverov, V. N.; Kobayashi, R.; Normand, J.; Raghavachari, K.; Rendell, A.; Burant, J. C.; Iyengar, S. S.; Tomasi, J.; Cossi, M.; Rega, N.; Millam, J. M.; Klene, M.; Knox, J. E.; Cross, J. B.; Bakken, V.; Adamo, C.; Jaramillo, J.; Gomperts, R.; Stratmann, R. E.; Yazyev, O.; Austin, A. J.; Cammi, R.; Pomelli, C.; Ochterski, J. W.; Martin, R. L.; Morokuma, K.; Zakrzewski, V. G.; Voth, G. A.; Salvador, P.; Dannenberg, J. J.; Dapprich, S.; Daniels, A. D.; Farkas, O.; Foresman, J. B.; Ortiz, J. V.; Cioslowski, J.; Fox, D. J. *Gaussian 09*; Gaussian, Inc.: Wallingford, CT, 2009.

(60) Bayly, C. I.; Cieplak, P.; Cornell, W.; Kollman, P. A. *J. Phys. Chem.* **1993**, *97*, 10269.

(61) Case, D. A.; Betz, R. M.; Cerutti, D. S.; Cheatham, T. E., III; Darden, T. A.; Duke, R. E.; Giese, T. J.; Gohlke, H.; Goetz, A. W.; Homeyer, N.; Izadi, S.; Janowski, P.; Kaus, J.; Kovalenko, A.; Lee, T. S.; LeGrand, S.; Li, P.; Luchko, T.; Luo, R.; Madej, B.; Merz, K. M.; Monard, G.; Needham, P.; Nguyen, H.; Nguyen, H. T.; Omelyan, I.; Onufriev, A.; Roe, D. R.; Roitberg, A.; Salomon-Ferrer, R.; Simmerling, C. L.; Smith, W.; Swails, J.; Walker, R. C.; Wang, J.; Wolf, R. M.; Wu, X.; York, D. M.; Kollman, P. A. *AMBER (2015)*; University of California: San Francisco, 2015.

(62) Darden, T.; York, D.; Pedersen, L. *J. Chem. Phys.* **1993**, *98*, 10089.

DOI: 10.1021/jacs.6b03774
J. Am. Chem. Soc. 2016, 138, 8184−8193